Influence of Alkali Metal Cations on the Rate of Oxygen Evolution from a Mixed Mg−$LiCoO_2$ Oxide

Leonardo Formaro* and Mariangela Longhi

Department of Physical Chemistry and Electrochemistry, University of Milan, Via Golgi 19, 20133 Milan, Italy

Received: December 12, 2002; In Final Form: February 27, 2003

O_2 evolution from a mixed Mg−$LiCoO_2$ oxide is investigated in base solutions of alkali metal cations (0.1−2 M LiOH, KOH, or CsOH) without added supporting electrolytes. Tafel slopes range 30−50 mV/decade, scarcely related to the used alkali. However, Tafel lines are displaced to more positive potentials in passing from CsOH to KOH and LiOH at the same concentration, and moreover, reaction orders with respect to OH^- decrease from ∼3 to ∼1 along the same alkali sequence with fractional rather than integer values. The reaction mechanism is examined on the assumption that Temkin-type adsorption conditions apply to the many reacting intermediates possibly involved. Analytical equations representing Tafel slope and reaction order in Temkin conditions are derived and reported for many frequently adopted O_2 evolution pathways, most of them for the first time. From these equations, the experimental behavior is reconciled with a constant mechanism (Kobussen's path) in which the rate-determining step varies depending on the alkali cation, shifting forward in the sequence of elementary steps from early positions in CsOH and KOH to the last one in which molecular O_2 is released in LiOH. Cation interactions with reacting surface sites apparently intervene to modify the reaction activation free energy profile, stronger for Li^+ than K^+ and Cs^+. Structural relations with Li^+ (and Mg^{2+}) sites in the oxide lattice may be involved. However, the interaction sequence, $Li^+ > K^+ > Cs^+$, is similar to that observed at the interface of many structurally and chemically unrelated oxides suspended in water and is attributed to entropic contributions from interactions of water molecules bonded in the hydration ion cosphere and at the oxide−solution interface.

Introduction

Transition metal oxides have widely acknowledged importance in electrocatalysis. Among others, most important achievements concern oxygen evolution catalysts. By extensively investigating oxide composition, structure, and binding techniques onto substrates, catalytic anodes have been developed over time allowing O_2 evolution to be modulated from barely detectable to quantitative depending on process requirements. Benefits in mass yield and energy consumption have been obtained together with most relevant improvements in plant design and reliability of a number of processes, such as chlorine evolution, water electrolysis, and metal electrowinning. Research still continues on dedicated anode materials.[1]

By comparison, electrolyte effects are far less investigated and reported. This is rather surprising and may suggest that, apart from a few well-known cases of strongly interacting anions (e.g., SO_4^{2-}, PO_4^{3-}), electrolyte ions behave nonspecifically with respect to the many reacting intermediates that form in any complex reaction and compete with one another for the available catalyst surface. However, changes in crystallographic radii and hydration make this position unlikely even for ions having closely comparable chemical features, such as the alkali metal cations.

The paper deals with O_2 evolution effects recorded on a Mg-doped lithium cobalt oxide (Mg−$LiCoO_2$) in LiOH, KOH, and CsOH in the absence of supporting electrolytes. KOH was used to establish a comparison with similar works on other oxide systems.[2−10] LiOH and CsOH were adopted to extend the previous data to solutions with different cation size and hydration. Variations in kinetic parameters (Tafel slope and mainly reaction order) have been observed well above statistical deviations.

Experimental Section

Magnesium-doped $LiCoO_2$ was prepared by thermal decomposition of Li_2CO_3, $MgCO_3$, and $Co(NO_3)_2 \cdot 6H_2O$. Reagents (Baker Analyzed) were ground in an agate mortar with a few drops of *n*-hexane added to form a thick paste. The mixture was dried at 70 °C for 1 h, heated at 300 °C (17 h), and finally annealed at 650 °C (54 h) in flowing O_2 with intermediate cooling and grinding. Reagents were dosed to correspond to 5 wt % Mg.

The product powder was characterized for phase purity by X-ray diffraction using a Siemens D500 apparatus in a 2θ range from 10° to 70° (0.02° steps, 1 s counting) and was found to closely correspond to nonsubstituted $LiCoO_2$ (JCPDS reference pattern 16-0427).

Electrodes were obtained as previously reported,[11] distributing comparably small oxide amounts (∼5 mg) onto both sides of thin Pt sheets (0.5×0.5 cm^2) painted with an electrochemically inactive graphite lacquer (Leit-C CCC, Neubauer Chemikalien, Germany) and evaporating solvents at room temperature. Electrodes with similar but not the same surface area result. In the lack of established criteria for real oxide surface area determination, results are presented as total current *E*/*I* (*E*/log(*I*)) relations relying on the observed electrode stability and self-consistent reproducibility. Further details are given when results are reported.

* To whom correspondence should be addressed. E-mail: formaro@icil64.cilea.it. Phone: 0039-02-50314229. Fax: 0039-02-50314300.

10.1021/jp027704a CCC: $25.00
Published on Web 06/05/2003

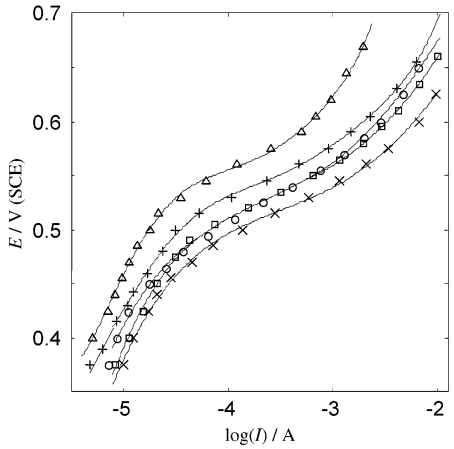

Figure 1. *E*/log(*I*) relations for O_2 evolution from Mg−$LiCoO_2$ at various molar LiOH concentrations: (△) 0.1; (+) 0.5; (○, □) 1; (×) 2 M. The symbols ○ and □ mark the first and last experimental run recorded on the single electrode used. $T = 25$ °C.

A three-electrode Pyrex cell with a Pt counter electrode and saturated calomel reference electrode (SCE, Amel, model 303/SCG/12 3P S7) were used. Electrolytes were prepared from doubly distilled water passed through a Milli-Q apparatus. LiOH, KOH (Baker Analyzed), and CsOH (Aldrich) were used as received. Measurements were carried out at 25 °C in still solutions kept under flowing O_2. A chain of analogue instruments was used (model 551 potentiostat, model 566 function generator, model 631 electrometer, Amel products), together with a digital acquisition system (Keithley Metrabyte DAS1802HR). Most often, currents became steady-state after 10−20 min from imposing each given potential. As reported in the paper, currents are averaged over 5 min of further recording at 600 Hz sampling rate. Potentials are reported on the experimental SCE scale after correcting for *IR* ohmic drops by a numerical method.[12]

Results and Discussion

Figure 1 shows several experimental curves recorded on a constant electrode at increasing alkali (LiOH) concentrations. *E*/log(*I*) coordinates are used. Each curve begins with a region of slowly increasing currents extending ∼100 mV positive with respect to spontaneous electrode potentials. Thereafter, short sections of linear Tafel relations appear, followed by gradually stronger bending upward at higher potentials.

Electrode stability and reproducibility readily emerge on the closely superimposing Tafel line sections independently recorded in 1 M LiOH, these having been obtained as the first and last experimental run of the used electrode, respectively. For control purposes, replicate *E*/*I* curves in 1 M alkali were similarly obtained on each used electrode and were adopted as a criterion to accept or discard results.

Deviations from Tafel lines at lower and higher potentials are apparent in the figure and are attributed to oxide passivation and uncompensated ohmic drops, respectively. These effects are separately considered because of their possible mechanistic implication.

Though involving small steady-state currents and weak potential dependence, the initial passivation process in Figure 1 is apparently a prerequisite for O_2 evolution and Tafel behavior to begin in LiOH, and in any investigated alkali as well. The process repeatedly occurs in each *E*/*I* curve, regardless of electrolyte concentration and previous electrode polarization at much more positive potentials. An unstable species has apparently to form by charge-transfer oxidation at the reacting oxide

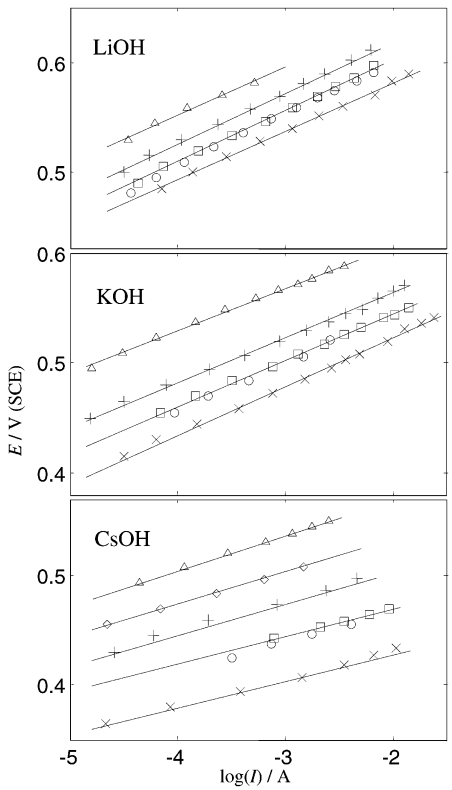

Figure 2. *IR*-corrected Tafel lines for O_2 evolution from Mg−$LiCoO_2$ at different concentrations of the indicated alkali: (△) 0.1; (◇) 0.2; (+) 0.5; (○, □) 1; (×) 2 M. The symbols ○ and □ show results of the first and last experimental run of used electrodes, respectively.

surface, spontaneously decaying backward by water contact when the electrical circuit is broken. Co^{4+} and related oxides may be such unstable products likely forming from Co^{3+} ions in the starting oxide stoichiometry. Unfortunately, no supporting evidence could be obtained on the subject by means of parallel voltammetric determinations, in which, despite wide scan rate variations, no anodic or cathodic maximum related to Co^{3+}/Co^{4+} electron transfer and Co^{4+} surface oxides could be detected against background currents of incipient O_2 evolution. Nevertheless, Co^{4+} likely forms during passivation and by similarity with other cobalt-based oxides may be assumed as the central cation of surface moieties behaving as intermediate reactants for O_2 evolution.

Uncompensated ohmic drops are, as a rule, due to linear current-dependent contributions from electrode and electrolyte resistance but may also conceal nonlinear terms due to changes in Tafel slope and films of gas bubbles that specifically intervene in gas-evolving reactions to better screen the effective surface area with increasing current density. *E*/*I* results were therefore carefully examined by means of independent numerical procedures, one of them based on usual trial-and-error calculations and a second one[12] directly providing resistance by means of $\Delta E/\Delta I$ vs $1/I$ plots constructed from experimental data. As discussed in the original paper,[12] this method allows linear and nonlinear ohmic drops to be readily distinguished. Consistent results were obtained by both techniques, showing comparable current-independent resistance calculated for each experimental run and cell arrangement ($R_\Omega \approx 4-30\ \Omega$, increasing with decreasing electrolyte concentration). As an example, the independent curves in 1 M LiOH in Figure 1 have uncorrected Tafel slopes of 50.8 ± 1.1 and 55.0 ± 0.3 mV/decade. Lower and less divergent values are obtained after *IR* correction (46.9 and 48.4 mV/decade, respectively; see also the related indistinguishable lines in Figure 2) by means of widely different

TABLE 1: Experimental Tafel Slopes and Reaction Orders for O_2 Evolution in 0.1−2 M LiOH, KOH, CsOH[a]

	$\partial E/\partial \log(I)$ (mV/decade)	reaction order with respect to OH^-
LiOH	50 ± 4	1.17 ± 0.06
	42 ± 4	1.16 ± 0.06
KOH	40 ± 4	1.76 ± 0.13
	39 ± 2	1.67 ± 0.13
CsOH	35 ± 5	2.86 ± 0.20
	29 ± 2	3.20 ± 0.29

[a] Each entry line shows results of an independent electrode.

TABLE 2: Calculated Reversible O_2 Evolution Potentials in 0.1 and 1 *m* Alkali

	0.1 *m*			1 *m*		
	E, V (SCE)	$\gamma_\pm$[a]	a_w	*E*, V (SCE)	$\gamma_\pm$[a]	a_w
LiOH	0.223	0.760	0.9968[b]	0.172	0.554	0.9696[b]
NaOH	0.223	0.766	*c*	0.165	0.678	0.8827[d]
KOH	0.222	0.798	*c*	0.163	0.756	0.9459[d]
CsOH	0.222	0.795	*c*	0.163	0.771	*e*

[a] Reference 13. [b] Reference 14. [c] Not available, assumed equal to a_w in 0.1 *m* LiOH [d] Reference 15. [e] Not available, assumed equal to a_w in 1 *m* KOH.

calculated R_Ω ($R_\Omega = 5.8$, $R_\Omega = 9.1\ \Omega$). No change in slope was detected up to the most positive range of potential on *IR*-corrected Tafel lines.

Figure 2 shows *IR*-corrected Tafel lines recorded on different alkali with comparable concentrations (0.1−2 M). Independent electrodes with variable surface area are used for each given alkali. Parallel lines appear with slopes that, by calculation, can be considered concentration-independent within standard deviations of at most a few millivolts (see Table 1). After averaging on concentration, we report Tafel slopes separately in Table 1 for each relevant alkali. To show further experimental reproducibility, comparatively small deviations appear between replicate results on independent electrodes.

As seen in Table 1, Tafel slopes range ∼30−50 mV/decade, scarcely related to the used alkali. However, electrolyte effects are evidenced by Tafel line positions, which shift to higher potentials in passing from LiOH to KOH and CsOH at corresponding concentrations. As a second feature, the concentration dependence of Tafel line separation is affected and remarkably increases along the same alkali sequence.

Variation in Tafel line potentials may contain thermodynamic contributions from variation in electrolyte and water activities, which are known to be specific functions of alkali concentration and nature. Reversible O_2 potentials were therefore calculated for 0.1 and 1 *m* solutions, the upper limit being the maximum concentration for which ionic coefficients could be found for CsOH.[13] Water activities are taken from refs 14 and 15 or are assumed as specified in the footnotes to Table 2 in which calculated reversible potentials are reported. Results weakly depend on the alkali nature, having a maximum difference of ∼10 mV observed between 1 *m* LiOH and 1 *m* CsOH. Greater potential differences are calculated from Tafel line potentials in 1 M LiOH and CsOH (90−110 mV depending on chosen current density), even though on a not exactly corresponding concentration scale. Shifts in Tafel line potentials are therefore considered to be true cation-dependent overpotential effects intervening to inhibit O_2 evolution.

Further electrolyte effects concern concentration-dependent Tafel line separation with varying alkali. The feature is unambiguously related to change in reaction order with respect to OH^-. The relevant Tafel data are in fact separately recorded on electrodes with a surface area that, though unknown, is reproducibly constant over the time scale necessary to obtain results in a given alkali (see comments to Figure 1).

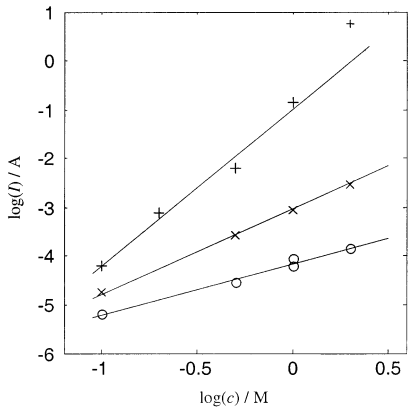

Figure 3. Variation of reaction orders with respect to OH^- with varying alkali: (○) LiOH; (×) KOH; (+) CsOH. $E = 0.500$ V/SCE; $T = 25$ °C. Results are obtained on a constant electrode for each investigated alkali.

Representative $\log(I)/\log(c_{OH^-})$ plots at a constant potential ($E = 0.500$ V/SCE) are reported in Figure 3 showing characteristic slopes that increase from ∼1 in LiOH to ∼1.7 in KOH and ∼3 in CsOH. Also keeping in account experimental scattering of replicate determinations on independent electrodes, Table 1 results suggest fractional rather than integer reaction orders.

Explanations for the described behavior were sought on the grounds of elementary paths that have been proposed over time to account for O_2 evolution features on one and another anode material. As originally proposed by Conway and co-workers,[16,17] Temkin-type isotherms were adopted to represent lateral interactions and coverage-dependent adsorption free energy of reacting surface intermediates. Langmuir adsorption behavior is in fact known for being incapable of justifying fractional reaction orders[16,18] at comparatively high electrolyte concentrations as experimentally used in the work. On this basis, kinetic equations were written down comprising a Butler−Volmer and an adsorption-related term. After elaboration, relations were obtained expressing Tafel slopes and reaction orders in closed analytical forms only containing an adsorption symmetry factor, δ, and the usual charge-transfer symmetry factor, α. Such equations are reported in Table 3 to permit comparison with previous treatments[16,18] and to extend available analytical solutions for some frequently adopted reaction paths[10,19−21] in Temkin-type conditions. To the best of our knowledge, analytical relations representing "Temkin" Tafel slopes and reaction orders are only available[16] for reaction paths C and D in Table 3. In another paper,[18] kinetic parameters for reaction paths in Table 3 were elaborated for Temkin conditions but were only reported as numerical data upon assuming specific charge-transfer symmetry factors, relative values of lateral interaction parameters of adsorbed species, and equilibrium constants of kinetically fast reactions taking place prior to the rate-determining step.

The presently adopted procedure and notation are shown in some detail by reference to Kobussen's path,[21] the second step being rate-determining. Up to this step, the path coincides with Bockris' "electrochemical" mechanism,[20] for which "Temkin" kinetic parameters are available in analytical form.[16] Similar equations were obtained for each following step of Kobussen's

TABLE 3: Diagnostic Criteria of Oxygen Evolution Reaction Paths Calculated for Temkin-type Adsorption Conditions[a]

rate-determining step	rds	ν		$(\partial E/\partial \ln(I))_{OH^-}$ (V/decade) NA	$(\partial E/\partial \ln(I))_{OH^-}$ (V/decade) A	reaction order with respect to OH^- NA	reaction order with respect to OH^- A
A. Krasil'shchikov's Path[b]							
(1) $M + OH^- \rightarrow MOH + e^-$	1	2		—		—	
(2) $MOH + OH^- \rightarrow MO^- + H_2O$	2	2		$(RT/F)(1-2\delta)^{-1}$		$2(1-\delta)$	
			$\delta \cong 0.5$	$(RT/F)(2(1-\delta))^{-1}$		$2(1-\delta)+1$	
(3) $MO^- \rightarrow MO + e^-$	3	2		$(RT/F)(2(1-\delta)-\alpha)^{-1}$		$1-2\delta$	
			$\delta \cong 0.5$	$(RT/F)(2(1-\delta)+1)^{-1}$		$2(1-\delta)+(1-\alpha)$	
(4) $2MO \rightarrow 2M + O_2$	4	1	$0.5 \cong \theta_{MO} \gg \theta_{MO^-}$	$(RT/F)2^{-1}$	$(RT/F)(2\delta^*)^{-1}$	2	$2\delta^*$
			$\theta_{MO} + \theta_{MO^-} = 0.5$, $\theta_{MO} \ll \theta_{MO^-}$	$(RT/F)4^{-1}$	$(RT/F)(2(1+\delta^*))^{-1}$	4	$2(1+\delta^*)$
B. O'Grady's Path[c]							
(1) $M^z + OH^- \rightarrow M^zOH + e^-$	1	2		—		—	
(2) $M^zOH \rightarrow M^{z+1}OH + e^-$	2	2		$(RT/F)(2(1-\delta)-\alpha)^{-1}$		$1-2\delta$	
			$\delta \cong 0.5$	$(RT/F)(2(1-\delta)+(1-\alpha))^{-1}$		$2(1-\delta)$	
(3) $2\,M^{z+1}OH + 2OH^- \rightarrow 2M^z + O_2 + 2H_2O$	3	1	$0.5 \cong \theta_{M^{z+1}OH} \gg \theta_{M^zOH}$	$(RT/F)2^{-1}$	$(RT/F)(2\delta^*)^{-1}$	4	$2(1+\delta^*)$
			$\theta_{M^{z+1}OH} + \theta_{M^zOH} = 0.5$, $\theta_{M^{z+1}OH} \ll \theta_{M^zOH}$	$(RT/F)4^{-1}$	$(RT/F)(2(1+\delta^*))^{-1}$	4	$2(1+\delta^*)$
C. Bockris' Electrochemical Path[d]							
(1) $M + OH^- \rightarrow MOH + e^-$	1	2		—		—	
(2) $MOH + OH^- \rightarrow MO + H_2O + e^-$	2	2		$(RT/F)(2(1-\delta)-\alpha)^{-1}$		$2(1-\delta)$	
			$\delta \cong 0.5$	$(RT/F)(2(1-\delta)+(1-\alpha))^{-1}$		$2(1-\delta)+1$	
(3) $2MO \rightarrow 2M + O_2$	3	1	$0.5 \cong \theta_{MO} \gg \theta_{MOH}$	$(RT/F)2^{-1}$	$(RT/F)(2\delta^*)^{-1}$	2	$2\delta^*$
			$\theta_{MOH} + \theta_{MO} = 0.5$, $\theta_{MO} \ll \theta_{MOH}$	$(RT/F)4^{-1}$	$(RT/F)(2(1+\delta^*))^{-1}$	4	$2(1+\delta^*)$
D. Bockris' Oxide Path[d]							
(1) $M + OH^- \rightarrow MOH + e^-$	1	4		—		—	
(2a) $2MOH \rightarrow MO + M + H_2O$	2a	2		$(RT/F)(2-3\delta)^{-1}$		$2-3\delta$	
(2b) $2MOH \rightarrow MOM + H_2O$	2b	2		$(RT/F)(2(1-2\delta))^{-1}$		$2(1-2\delta)$	
			$\delta \cong 0.5$	$(RT/F)(4(1-\delta))^{-1}$		$4(1-\delta)$	
(3) $2MO \rightarrow 2M + O_2$	3	1	$0.5 \cong \theta_{MO} \gg \theta_{MOH}$	$(RT/F)2^{-1}$	$(RT/F)(2\delta^*)^{-1}$	2	$2\delta^*$
			$\theta_{MOH} + \theta_{MO} = 0.5$, $\theta_{MO} \ll \theta_{MOH}$	$(RT/F)4^{-1}$	$(RT/F)(2(1+\delta^*))^{-1}$	4	$2(1+\delta^*)$
E. Kobussen's Path[e]							
(1) $M + OH^- \rightarrow MOH + e^-$	1	1		—		—	
(2) $MOH + OH^- \rightarrow MO + H_2O + e^-$	2	1		$(RT/F)(2(1-\delta)-\alpha)^{-1}$		$2(1-\delta)$	
			$\delta \cong 0.5$	$(RT/F)(2(1-\delta)+(1-\alpha))^{-1}$		$2(1-\delta)+1$	
(3) $MO + OH^- \rightarrow MO_2H^-$	3	1		$(RT/F)(1-2\delta)^{-1}$		$2(1-\delta)$	
			$\delta \cong 0.5$	$(RT/F)(3-2\delta)^{-1}$		$2(1-\delta)+2$	
(4) $MO_2H^- + OH^- \rightarrow MO_2^- + H_2O + e^-$	4	1		$(RT/F)((2(1-\delta)-\alpha)^{-1}$		$2(1-\delta)$	
			$\delta \cong 0.5$	$(RT/F)(2(1-\delta)+(2-\alpha))^{-1}$		$2(1-\delta)+3$	
(5) $MO_2^- \rightarrow M + O_2 + e^-$	5	1	$0.5 \cong \theta_{MO_2^-} \gg \theta_{MO_2H^-}$	$(RT/F)(2-\alpha)^{-1}$	$(RT/F)((1-\alpha)+\delta^*)^{-1}$	1	δ^*
			$\theta_{MO_2^-} + \theta_{MO_2H^-} = 0.5$, $\theta_{MO_2^-} \ll \theta_{MO_2H^-}$	$(RT/F)(3-\alpha)^{-1}$	$(RT/F)((2-\alpha)+\delta^*)^{-1}$	2	$1+\delta^*$

[a] δ, symmetry factor of adsorption; δ^*, symmetry factor of molecular oxygen desorption; α, symmetry factor of charge transfer, usually equal to δ;[17] ν, stoichiometric number; —, left undetermined because of the unresolvable analytical dependence of θ on I and E; NA, nonactivated, and A, activated, desorption of molecular O_2. [b] Reference 19. [c] Reference 10. [d] Reference 20. [e] Reference 21.

path being rate-determining and are reported in Table 3. The treatment is available as Supporting Information.

Kobussen's path begins by the following consecutive steps:

$$M + OH^- \rightarrow MOH + e^- \quad (1)$$

$$MOH + OH^- \rightarrow MO + H_2O + e^- \quad (2)$$

If step 2 is rate-determining, the current rate equation is

$$I = F\vec{k}_2\theta_{MOH}c_{OH^-}\exp\left((1-\alpha)\frac{EF}{RT}\right) \times \exp\left(-\delta\frac{f(\theta)}{RT} + (1-\delta)\frac{f(\theta)}{RT}\right) \quad (3)$$

where θ_{MOH} is the surface coverage of adsorbed MOH, c_{OH^-} is the alkali concentration, and $\vec{k}_2$ is the forward rate constant. F, R, T, and E have usual meanings. Most relevant to Temkin conditions, $f(\theta)$ is assumed,[22] with the form $f(\theta) = \sum_i g_i\theta_i$, to represent coverage-dependent deviations in adsorption free energy, ΔG_θ, from Langmuir conditions, $\Delta G_\theta = \Delta G_0 + f(\theta)$, at a total surface coverage, θ, as it results from individual contributions of several surface intermediates possibly involved. This is by analogy with adsorption of a single intermediate,[17,22-24] $\Delta G_\theta = \Delta G_0 + f(\theta) = \Delta G_0 + g\theta$, where g is a lateral interaction parameter, positive or negative for repulsive or attractive interactions, respectively. δ ($0 < \delta \leq 1$) is a symmetry factor for a forward adsorption process, which depends in magnitude on the form of the activation energy barrier[17] and is usually equal to the charge-transfer symmetry factor, α.[17] As used here, δ and α substitute $(1-\gamma)$ and $(1-\beta)$ in ref 16.

The term $\exp(-\delta(f(\theta)/(RT)) + (1-\delta)(f(\theta)/(RT)))$ in eq 3 takes into account any variation in adsorption free energy from the initial (MOH, $(1-\delta)(f(\theta)/(RT))$) to the final state (MO,

$-\delta(f(\theta)/(RT))$) of reaction 2, as it results from variations in total coverage with applied potential.[16,17,23,24]

Even in the lack of knowledge of individual g_i, a relation is obtained for $f(\theta)$ on the assumption that quasi-equilibrium is established between forward and backward reactions 1:

$$f(\theta) = RT \ln\left(\frac{\vec{k}_1}{\overleftarrow{k}_1}\frac{\theta_M}{\theta_{MOH}}\right) + RT \ln c_{OH^-} + EF \qquad (4)$$

which can be substituted in eq 3,

$$\ln I = \text{const} + 2(1-\delta)\ln c_{OH^-} + \ln \theta_{MOH} + (2(1-\delta)-\alpha)\frac{EF}{RT} \qquad (5)$$

where $\ln \theta_{MOH}$ is negligible at intermediate coverage and is therefore omitted.[17,24] const is a sum of terms:

$$\text{const} = \ln(F\vec{k}_2) + (1-2\delta)\ln\left(\frac{\vec{k}_1}{\overleftarrow{k}_1}\right) + (1-2\delta)\ln\frac{\theta_M}{\theta_{MOH}}$$

where $\ln \theta_M/\theta_{MOH}$ is relatively constant[16] and negligible at intermediate coverages.

For step 2, rate-determining Tafel slope and reaction order follow from eq 5:

$$\left(\frac{\partial E}{\partial \ln I}\right)_{c_{OH^-}} = \frac{1}{(2(1-\delta)-\alpha)}\frac{RT}{F};\quad \left(\frac{\partial \ln I}{\partial \ln c_{OH^-}}\right)_E = 2(1-\delta) \qquad (6)$$

These relations are the same as those for Bockris' "electrochemical" path.[16] Other relations were obtained assuming that each step in Kobussen's path is rate-determining and are reported in Table 3 (see also the Supporting Information for derivation details).

Inspection of Table 3 readily shows that, with the single exception of Krasil'shchikov's path, reaction orders are single-valued functions of δ alone. Therefore, the parameter is unambiguously obtained experimentally. Moreover, as stated above, δ is equal to α, so that Tafel slopes can be calculated for each presumably relevant path and rate-determining step and can be compared with corresponding experimental data in a matter of self-consistency and physical likelihood of both parameters δ and α. Though straightforward, the procedure may look somewhat formal and abstract. However, a physical picture emerges from δ. Depending on the coefficient magnitude, the shape of the rate-determining step (rds) energy barrier can be inferred to show whether the reaction is preferentially shifted toward reactants ($\delta > 0.5$) or products ($\delta < 0.5$) without assumptions on the reaction rate constant. This aspect is considered further for the case that release of molecular oxygen is rate-determining (step 5 of path E in Table 3; see LiOH results below and Supporting Information in a general form).

CsOH. In CsOH, Tafel slopes and reaction orders with respect to OH^- range 29−35 mV/decade and 2.86−3.20, respectively, depending on the electrode response (see Table 1). From Table 3, a single mechanism is in accordance with results, namely, Kobussen's path (path E) with the third step being rate-determining: $MO + OH^- \rightarrow MO_2H^-$. Satisfactory agreement is observed between experimental and calculated data (see Table 4). The value of δ is ∼0.5, indicating a nearly symmetrical activation energy barrier between the involved reactants, MO and MO_2H^-.

TABLE 4: Comparison of Experimental and Calculated Tafel Slopes for Kobussen's Path in Temkin-type Conditions[a]

	exptl reaction order with respect to OH^-	rds	δ	$\partial E/\partial \log (I)$ (mV/decade) calcd	exptl
LiOH	1.17	fifth	0.17[b]	44	50
	1.16		0.16[b]	45	42
KOH	1.76	second or fourth	0.12	36	40
	1.67		0.16	39	39
CsOH	2.86	third	0.57	32	35
	3.20		0.40	27	29

[a] Experimental reaction orders are used to calculate symmetry factors, δ, and Tafel slopes of proposed rate-determining steps for O_2 evolution in different alkali. [b] $\delta = \delta^*$.

KOH. Tafel slope and reaction order with respect to OH^- are 39−40 mV/decade and 1.67−1.76, respectively (Table 1). These values may correspond to (a) Bockris' "electrochemical" path (Table 3, path C) with the second step being rate-determining, (b) Kobussen's path (path E) with the second step being rate-determining ($MOH + OH^- \rightarrow MO + H_2O + e^-$), and (c) Kobussen's path (path E) with the fourth step being rate-determining ($MO_2H^- + OH^- \rightarrow MO_2^- + H_2O + e^-$). Cases a and b coincide up to the rds with no distinction possible and necessary between them. However, in Bockris' "electrochemical" path, oxygen release (step 3 of path C in Table 3) is a bimolecular reaction involving concerted recombination of radicals from adjacent surface sites, MO. This is considered to make the mechanism scarcely probable.[18] Thus cases b and c likely apply.

In Table 4, calculated parameters for cases b and c closely agree with one another and with experimental data. In each case δ is <0.5, showing that each relevant rate-determining step is shifted forward, toward formation of either MO (case b) or MO_2^- (case c).

LiOH. Tafel slope and reaction order are 42−50 mV/decade and 1.16−1.17, respectively (Table 1). By comparison with Table 3, a single path can account for experimental parameters, namely, Kobussen's path E with step 5 being rate-determining: $MO_2^- \rightarrow M + O_2 + e^-$, where molecular O_2 eventually forms by an activated desorption process also involving $\theta_{MO_2^-} \ll \theta_{MO_2H^-}$ and $\theta_{MO_2^-} + \theta_{MO_2H^-} \cong 0.5$. For activated desorption, rather than adsorption as so far assumed, the symmetry factor δ is redefined as δ^* [17] and the charge-transfer symmetry factor, α, is substituted by $1 - \delta^*$ [17] (see Table 3). Moreover, additional specifications are introduced[16,17] that (a) oxygen desorption is activated if $\delta^* \neq 1$ and (b) oxygen desorption is favored for $\delta^* > 0.5$. Experimental data reasonably agree with calculated values (Table 4). The value of δ^* is lower than 0.5, showing that oxygen desorption is activated and shifted to the left. Moreover, $\theta_{MO_2^-} \ll \theta_{MO_2H^-}$ reveals that the preceding quasi-equilibrium step has an electrochemical constant appreciably less than unity.[16]

From the preceding results and elaboration, a single multistep path is involved with one or another elementary step behaving as rds in relation to the present alkali cation.

As seen from reversible potentials in Table 2, the reaction free energy, from reacting OH^- [18] to molecular O_2, is essentially cation-independent in 0.1 *m* electrolytes and varies by ∼10 mV from 1 *m* LiOH to 1 *m* CsOH. The total reaction free energy can be considered nearly constant, comprised of the constant free energy state of the end reaction product molecular O_2 and the nearly constant state of reacting OH^-. Cation interactions have to occur to modify the activation free energy maximum

of any relevant elementary step comprised in the elementary sequence. The free energy of surface sites would decrease by spontaneous ion interaction, causing a proportional decrease of the activation energy barrier between reactant surface sites possibly affected by ion interaction. A change in rds may occur depending on the relative height of activation free energy maxima, as measured from the initial state of OH^-.[25]

In this picture, Li^+ is the strongest interacting cation, having interaction energies large enough to stabilize all reactive intermediates such that the highest free energy maximum in the barrier is that of the last kinetic step, which has to tail off at the fixed thermodynamic end point of the barrier, where molecular O_2 is desorbing. K^+ and Cs^+ behave similarly but more weakly, selectively stabilizing any surface intermediate reacting in the experimental rds (namely, the third step in CsOH and the second (or fourth) one in KOH) rather than in preceding and following steps.

From comparatively strong and indiscriminate in LiOH, ion interactions become weaker and specific in CsOH and KOH, in this providing distinctive chemical evidence for the many groups formally adopted in Kobussen's mechanism.

Alkali cation effects were already reported for O_2 evolution from oxidized cobalt metal[26] with, in that case, $\eta_{LiOH} > \eta_{NaOH} > \eta_{KOH}$ at high electrolyte concentration (e.g., 2.5 M) and $\eta_{NaOH} > \eta_{KOH} > \eta_{LiOH}$ in 0.1 M alkali with a further dependence observed on current density. The effect was attributed to cation penetration into outermost oxide layers. Though not excluding that similar processes also occur on the present oxide, other factors of a more general nature can be considered with so far scarcely explored effects on oxide charge-transfer behavior. Ion interaction/adsorption sequences similar to the present one, $Li^+ > K^+ > Cs^+$ (Li > Cs, for brevity in the following), have been reported for the interfacial behavior of several unrelated oxides (TiO_2, Fe_2O_3, Al_2O_3)[27−31] suspended in water. Opposite ion sequences (Cs > Li)[28,32] are actually also reported for similar oxides, mainly differing by better crystallinity, surface order, and state. Structural oxide factors are therefore not exclusive for the observed behavior. Entropic factors are instead mainly involved in controlling ion adsorption and separately concern water order/disorder in the hydration cosphere of interacting ions and at the oxide−solution interface. Li^+ is the strongest "order producing"[33] ion in the alkali metal cation series, K^+ and Cs^+ behaving as gradually stronger "order destroying"[33] ions. For entropic reasons,[33,34] Li^+ and Cs^+ can be expected to more favorably interact with surfaces having similar "order producing" and "order destroying" behavior, respectively. By model simulations,[29] low and high inner layer capacitance values have been determined as a discriminating factor between order/disorder water states and Li > Cs or Cs > Li ion adsorption sequences. Transition from low to high capacitance values can be assumed to represent a changeover from ordered to disordered adsorbed water layers. This also acts in favor of Cs > Li, rather than Li > Cs, adsorption ion sequences.[27−31,35] This latter case (Li > Cs) is in accordance with the present results.

Acknowledgment. Financial support from the Ministry of Education, University, and Research (MIUR) and from the National Council of Research (CNR) is gratefully acknowledged.

Supporting Information Available: Detailed mathematical treatment of Kobussen's pathway. This material is available free of charge via the Internet at http://pubs.acs.org.

Note Added after ASAP Posting. This article was released ASAP on 6/5/2003 with incorrect axis labels on Figure 3. The correct version was posted on 6/20/2003.

References and Notes

(1) Chen, G.; Chen, X.; Yue, P. L. *J. Phys. Chem. B* **2002**, *106*, 4364.
(2) Willems, H.; Kobussen, A. G. C.; De Wit, J. H. W.; Broers, G. H. J. *J. Electroanal. Chem.* **1984**, *170*, 227.
(3) Willems, H.; Kobussen, A. G. C.; Vinke, I. C.; De Wit, J. H. W.; Broers, G. H. J. *J. Electroanal. Chem.* **1985**, *194*, 287.
(4) Efremov, B. N.; Tarasevich, M. R. *Elektrokhimiya* **1981**, *17*, 1672.
(5) Švegl, F.; Orel, B.; Grabec-Švegl, I.; Kaučič, V. *Electrochim. Acta* **2000**, *45*, 4359.
(6) Bronoel, G.; Reby, J. *Electrochim. Acta* **1980**, *25*, 973.
(7) Rasiyah, P.; Tseung, C. C. *J. Electrochem. Soc.* **1984**, *131*, 803.
(8) Rasiyah, P.; Tseung, C. C.; Hibbert, D. B. *J. Electrochem. Soc.* **1982**, *129*, 1724.
(9) Singh, R. N.; Hamdani, M.; Koenig, J. F.; Poillerat, G.; Gautier, J. L.; Chartier, P. *J. Appl. Electrochem.* **1990**, *20*, 442.
(10) O'Grady, W.; Iwakura, H. J.; Yeager, E. In *Electrocatalysis*; Breiter, M. W., Ed.; The Electrochemical Society: Princeton, NJ, 1974; p 286.
(11) Longhi, M.; Formaro, L. *J. Electroanal. Chem.* **1999**, *464*, 149.
(12) Krstajic, N.; Trasatti, S. *J. Appl. Electrochem.* **1998**, *28*, 1291.
(13) Conway, B. E. *Electrochemical Data*; Elsevier Publishing Co.: Amsterdam, NL, 1952; pp 75−78.
(14) Chouaib, F.; Delgado-Paniagua, G.; Picard, G. *J. Chim. Phys.* **1988**, *85*, 627.
(15) Chouaib, F.; Gomez-Pedrozo, A.; Picard, G. *J. Chim. Phys.* **1987**, *84*, 489.
(16) Conway, B. E.; Salomon, M. *Electrochim. Acta* **1964**, *9*, 1599.
(17) Gileadi, E.; Conway, B. E. In *Modern Aspects of Electrochemistry*; Bockris, J. O'M., Conway, B. E., Eds.; Butterworth: London, U.K., 1964; Vol. 3, p 347.
(18) Bockris, J. O'M.; Otagawa, T. *J. Phys. Chem.* **1983**, *87*, 2960.
(19) Krasil'shchikov, A. I. *Russ. J. Phys. Chem.* **1963**, *37*, 273.
(20) Bockris, J. O'M. *J. Chem. Phys.* **1956**, *24*, 817.
(21) Kobussen, A. G. C.; Broers, G. H. J. *J. Electroanal. Chem.* **1981**, *126*, 221.
(22) Conway, B. E.; Gileadi, E. *Trans. Faraday Soc.* **1962**, *58*, 2493.
(23) Thomas, J. G. N. *Trans. Faraday Soc.* **1961**, *57*, 1603.
(24) Parsons, R. *Trans. Faraday Soc.* **1958**, *54*, 1053.
(25) Bockris, J. O'M. In *Modern Aspects of Electrochemistry*; Bockris, J. O'M., Ed; Butterworth: London, U.K., 1954; Vol. 1, p 180.
(26) Tur'yan, Ya. I.; Gershkovich, I. A. *Russ. J. Phys. Chem.* **1961**, *35*, 925.
(27) Bérubé, Y. G.; De Bruyn, P. L. *J. Colloid Interface Sci.* **1968**, *28*, 92.
(28) Dumont, F.; Warlus, J.; Watillon, A. *J. Colloid Interface Sci.* **1990**, *138*, 543.
(29) Bourikas, K.; Hiemstra, T.; Van Riemsdijk, W. H. *Langmuir* **2001**, *17*, 749.
(30) Dumont, F.; Watillon, A. *Discuss. Faraday Soc.* **1971**, *52*, 353.
(31) Breeuwsma, A.; Lyklema, J. *Discuss. Faraday Soc.* **1971**, *52*, 324.
(32) Fokkink, L. G. J.; De Keizer, A.; Lyklema, J. *J. Colloid Interface Sci.* **1989**, *127*, 116.
(33) Gurney, R. W. *Ionic Processes in Solution*; Dover Publications: New York, 1962.
(34) Lyklema, J. *Mol. Phys.* **2002**, *100*, 3177.
(35) Sprycha, R. *J. Colloid Interface Sci.* **1984**, *102*, 173.